

Development of micro-vibrating flow pumps using MEMS technologies

Osman Omran Osman · Hirofumi Shintaku ·
Satoyuki Kawano

Received: 1 March 2012 / Accepted: 24 April 2012 / Published online: 10 May 2012
© The Author(s) 2012. This article is published with open access at Springerlink.com

Abstract In the present paper, we propose a micro-vibrating flow pump (micro-VFP), which is a novel micropump. The micro-VFP is constructed using an actively vibrating valve that has a cantilever-like structure fixed on a wall of a microchannel and a slit orifice downstream. The slit orifice is designed to make the flow asymmetric around the vibrating valve and to effectively generate a net flow in one direction. At the same time, the valve works as an actuator to induce liquid flow in the microchannel. Since the valve is made of a flexible material including magnetic particles, it is manipulated by changing the magnetic field from outside the micro-VFP. This design allows external operation of the micro-VFP without any electrical or mechanical connections. In addition, the micro-VFP, which realizes pumping with a chamber free design, is advantageous for implementation in a small space. In order to demonstrate its basic pumping performance, a prototype micro-VFP was fabricated in a microchannel with a cross section of $240\ \mu\text{m} \times 500\ \mu\text{m}$ using microelectromechanical systems technologies. The vibration characteristics of the valve were investigated using a high-speed camera. The pump performance at various actuation frequencies in the range of 5 to 25 Hz was evaluated by measuring the hydrostatic head and the flow rate. The proposed micro-VFP design exhibited an increase in performance with the driving frequency and had a maximum shut-off pressure of $3.8 \pm 0.4\ \text{Pa}$ and a maximum flow rate of $0.38 \pm 0.02\ \mu\text{l}/\text{min}$ at 25 Hz. Furthermore, in order to clarify the

detailed pumping process, the flow characteristics around the vibrating valve were investigated by analyzing the velocity field based on micron-resolution particle image velocimetry (micro-PIV). The validity of the hydrostatic measurement was confirmed by comparing the volume flow rate with that estimated from micro-PIV data. The present study revealed the basic performance of the developed micro-VFP.

Keywords Micropump · Vibrating flow pump · Valve · MEMS · Micro-PIV

1 Introduction

Many technologies for micro-biochemical analysis systems, referred to as micro-total analysis systems (Manz et al. 1990) or lab on a chip (Stone et al. 2004), have been developed in recent decades. In these systems, fluid transportation, mixing, biochemical reactions, separation and detection are automatically carried out using a small amount of sample fluids and reagents. The confinement effect by the microchannel results in the uniformity of reactions. Therefore, these systems have numerous advantageous features, such as reduced analysis time, total cost, and patient pain. For the development of reliable and fully automated systems, various micropumps, which are a key technology for transporting fluids at high pressure due to the very small cross section of the microchannel, i.e., head loss, have been proposed (Peter 2005). Previous micropumps can be roughly divided into two categories: mechanical pumps and nonmechanical pumps. The first category usually realizes pumping by pressurizing the working fluid using check valves, oscillating membranes, or turbines (van Lintel et al. 1988). The second category

O. O. Osman · H. Shintaku · S. Kawano (✉)
Department of Mechanical Science and Bioengineering,
Graduate School of Engineering Science, Osaka University,
1-3 Machikaneyama, Toyonaka, Osaka 560-8531, Japan
e-mail: kawano@me.es.osaka-u.ac.jp

adds momentum to the fluid by converting another energy form into kinetic energy. Typical pumps belonging to this category are electrohydrodynamic micropumps (Bart et al. 1990), electroosmotic micropumps (Liu and Dasgupta 1992), and magnetohydrodynamic pumps (Jang and Lee 2000). However, most current micropumps do not satisfy the requirements for lab on a chip, such as precise control of a small flow rate, in the range of microliters per minute or less, because the size of the present micropumps is relatively large or because of the lack of a stable pumping mechanism.

The vibrating flow pump (VFP), which, at present, is a macroscale pump, was first proposed by Hashimoto et al. (1994). The working principle of the VFP is to provide kinetic energy to the working liquid by vibrating a liquid column in a tube with a valve on its side. The VFP has many advantageous features such as an extremely simple structure, self-priming, and controllability of the pumping performance. The VFP has received considerable attention in various industrial fields of mechanical and chemical engineering because of the above advantages. Furthermore, the VFP has been considered to be a suitable mechanism for the left ventricular assist device (LVAD) in the field of artificial organs (Yambe et al. 2003; Kawano et al. 2001; Shintaku et al. 2010) because the VFP can stably generate an oscillating flow with various frequencies. The miniaturized VFP, which is a millimeter-order pump, was introduced by Kawano et al. and proposed for use as a booster pump for the external shunt catheter in clinical applications (Kawano et al. 2003; Kato et al. 2003). However, application of the VFP to microfluidic systems requires further miniaturization.

In the present study, we have developed a micro-VFP fabricated by microelectromechanical systems (MEMS) technology (Shintaku et al. 2007, 2008; Inaoka et al. 2011) in order to apply VFP to the application of micro-total analysis systems or lab on a chip. In contrast to vibrating a tube in a macro-scale VFP, we vibrate the valve in a micro-VFP. This modification, vibrating the thin plate valve instead of the tube, one side of which is fixed to the channel wall, contributes to a dramatic decrease in size and power consumption. This novel pump is realized primarily by the development of a vibrating valve made of polydimethylsiloxane (PDMS), including magnetic particles to manipulate the valve from outside the pump. The pumping performance was investigated by measuring the hydrostatic head generated at various driving frequencies. Furthermore, the fluid dynamics in the micro-VFP were achieved by a noncontact flow observation based on micron-resolution particle image velocimetry (micro-PIV). The micro-VFP could precisely control the flow rate in the range of 0.07 ± 0.02 to 0.38 ± 0.02 $\mu\text{l}/\text{min}$. Therefore, the micro-VFP is useful for accurate control of small amounts of fluid

used in applications such as single-molecule studies (Perkins et al. 1995; Nagahiro et al. 2007; Hanasaki et al. 2008; Doi et al. 2010). The maximum pressure was 3.8 ± 0.4 Pa, which was sufficiently high to transport the liquid through the micro-scaled channels. The results obtained herein provide a basic understanding of the pumping performance of the micro-VFP.

2 Structure of micro-VFP

Figure 1a shows a schematic diagram of the micro-VFP and the concept of the pumping operation. The micro-VFP consists of a cantilever-like vibrating valve and a slit orifice downstream. As a result of the asymmetric vibration of the valve between upstream and downstream, and the asymmetric structure due to the combination of the slit orifice and the valve, the micro-VFP generates one-directional flow in the microchannel by providing kinetic energy to the working fluid. Since the valve is made of a flexible material, e.g., PDMS, including magnetic particles, the micro-VFP can be externally operated only by changing the magnetic field in the vicinity of the valve. Therefore, no electrical or mechanical connections are needed. In addition, compared with the conventional micropump based on a chamber with a diaphragm (van Lintel et al. 1988), the micro-VFP is relatively small for incorporation into a microchannel.

Figure 1b shows a three-dimensional illustration of the micro-VFP and the dimension of the structure. Note that the flow direction is opposite to that in Fig. 1a in order to show the details of the vibrating valve and the cross section of the microchannel. The valve is designed as a cantilever-like structure fixed to the wall of a microchannel. The valve is a relatively high-aspect-ratio structure, with a thickness of 40 μm , a width of 200 μm , and a height of 490 μm , in order to make the valve flexible enough to vibrate. The valve is located at the center of the microchannel, which has a width of 240 μm , a depth of 500 μm , and a length of 5.3 mm. Small clearances between the valve and the walls are designed with ends of 10 μm and sides of 20 μm . A slit orifice is designed 50 μm downstream from the valve with a gap of 50 μm . A schematic diagram of the actuation of the vibrating valve using an outside permanent magnet (PM) is shown in Fig. 1c. The motion of the PM changes the magnetic field in the vicinity of the valve. The valve is deformed upstream taking a new position when the edge of the PM is located on the upstream side of the valve as a result of the attractive force. The valve vibrates around the new oscillation center according to the PM, due to the oscillation of the magnetic field. Consequently, the vibration of the PM results in periodic asymmetric vibration of the valve.

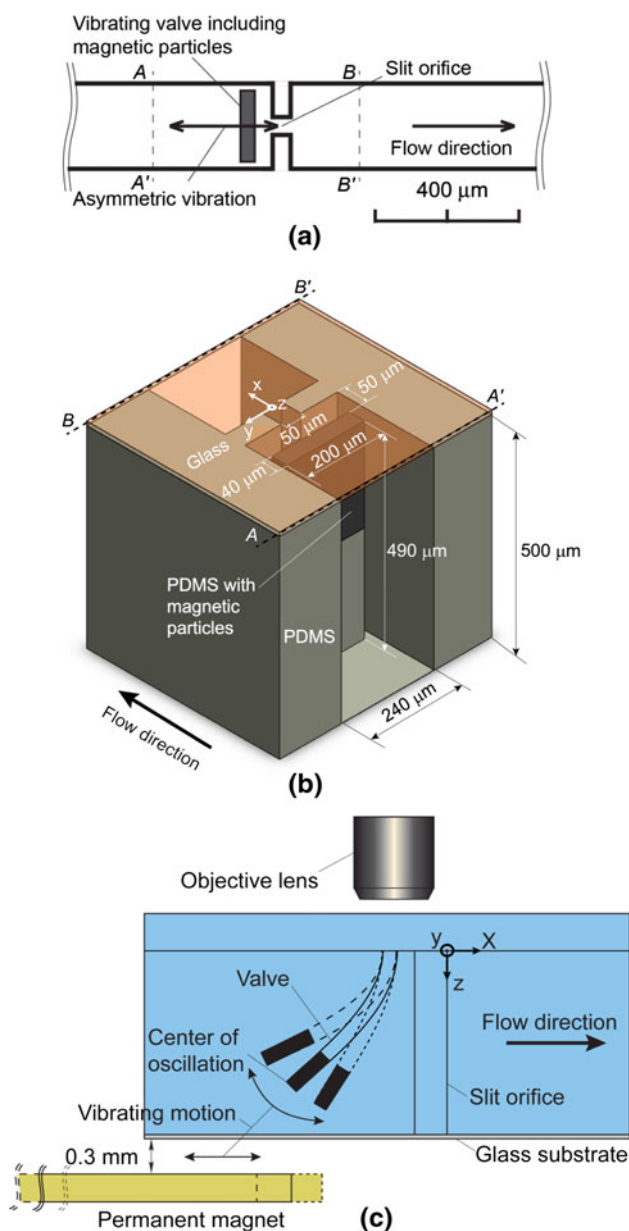


Fig. 1 **a** Schematic diagram of pumping of the micro-VFP, **b** the dimensions of the structure around the vibrating valve, and **c** schematic diagram of the actuation of the vibrating valve using an outside permanent magnet

3 Fabrication

Figure 2 shows a schematic diagram of the fabrication procedure. We developed an optimized process conditions for the SU-8 mold, as described in Table 1 to achieve the relatively high-aspect-ratio structure of the micro-VFP. The SU-8 mold had two layers with thicknesses of 10 and 500 μm to fabricate a clearance between the valve tip and the microchannel wall. The fabrication processing sequence is as below:

- (a) A silicon wafer was cut into square substrates having sides of 3 cm.
- (b) Al thin film was deposited on the substrate by radio-frequency magnetron sputtering in order to facilitate the subsequent alignment process.
- (c) A 10-μm thick layer of SU-8 (SU-8 3005, MicroChem, USA) was coated on the Al surface using a spinner and was patterned by standard UV lithography for the fabrication of the clearance between the tip of the valve and the microchannel wall.
- (d) Development of SU-8.
- (e) Except for the region of the clearance and the cross marks, the Al thin film was etched by a wet process. The 10-μm thick SU-8 layer for the clearance worked as an etching mask in this process. The cross marks helped in the alignment process because the color of the Al was different from that of the silicon substrate. The surface was then coated with an adhesion promoter (Omnicat™, MicroChem, USA).
- (f) A 500-μm thick SU-8 (SU-8 2150, MicroChem, USA) was formed over the substrate using a spinner and was patterned to form the structure of the mold.
- (g) Development of SU-8.
- (h) The SU-8 mold was used to form the PDMS into the structure of the micro-VFP. The surface of the SU-8 mold was pretreated with a barrier coat (barrier coat No. 6, Shin-Etsu Chemical Co., Ltd., Japan) in order to enhance the removal of the PDMS from the mold. A liquid PDMS (Sylgard® 184, DowCorning, USA) was mixed with a curing agent at a volume concentration of 10 % and was degassed in a vacuum before being cast over the mold. In addition, we prepared a liquid PDMS including magnetic particles of iron oxide with a diameter of 1 μm (Fe₃O₄, Kojundo Chemical Lab Co., Ltd.). The volume concentration of the particles in liquid PDMS was 25 %. We manually placed a drop of the liquid PDMS including magnetic particles into the hole for the fabrication of the vibrating valve in the mold. The liquid PDMS without magnetic particles was then cast over the entire area of the mold. The mold with the PDMS was then placed on a hot plate at 65 °C for 45 min to cure.
- (i) The cured PDMS was removed from the mold, and two holes with diameters of 1.0 mm were punched as a flow inlet and a flow outlet at the ends of the microchannel, as shown in Fig. 2i.

The micro-VFP fabricated by the PDMS was sealed with a 1-mm thick glass substrate (Matsunami Glass Ind., Ltd., Japan) by oxygen plasma bonding (Kim et al. 2004). The bonding process started from the plasma treatment on the surface of the PDMS and the glass substrate under a pressure of 26.3 Pa and a power of 100 W for 30 s. The

Fig. 2 Fabrication process of the two-layered SU-8 mold: **a** silicon substrate, **b** Al thin film deposition using radiofrequency magnetron sputtering, **c** spin coating and patterning of a 10- μm thick layer of SU-8 for clearance, **d** development of SU-8, **e** etching Al thin film for alignment, **f** spin coating and patterning of a 500- μm thick SU-8 layer, **g** development of SU-8, **h** pouring PDMS onto the SU-8 mold, and **i** punching holes for the inlet and the outlet in PDMS

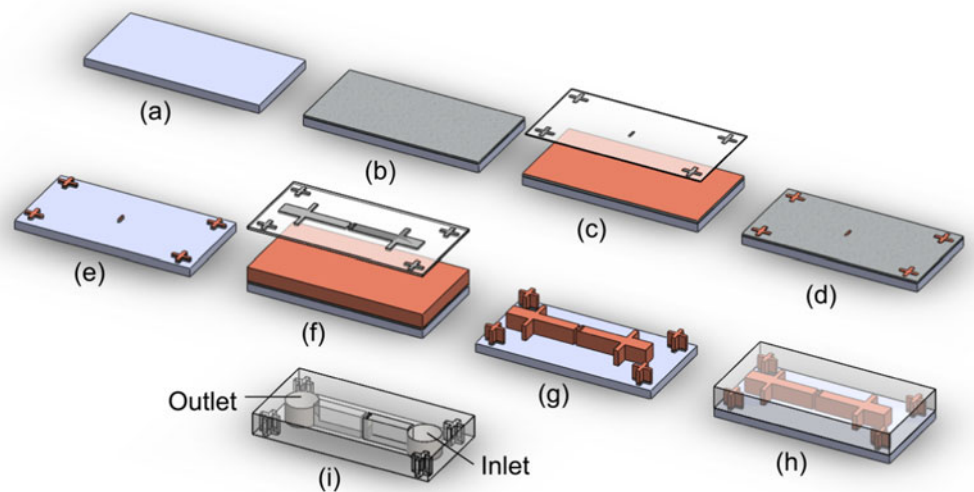


Table 1 Comparison of fabrication processes for a mold with high-aspect-ratio structure using SU-8 2150

	Standard process	Optimized process
Spin coating	5 s at 500 rpm	5 s at 500 rpm
	30 s at 1,300 rpm	30 s at 1,300 rpm
Soft baking	10 min at 65 °C	1 h at 65 °C
	120 min at 95 °C	4 h at 95 °C
Exposure energy	600 mJ/cm ²	800 mJ/cm ² divided four times
Post exposure bake	5 min at 65 °C	1 h at 65 °C
	30 min at 95 °C	2 h at 95 °C
		13 h at 60 °C
Development	28 min	60 min

PDMS and the glass substrate were then immediately assembled and baked on a hot plate at 70 °C for 30 min.

Figure 3 shows SEM images of the resultant PDMS structure around the vibrating valve. Using the optimized process parameters described above, we successfully achieved the fabrication of a relatively high-aspect-ratio structure. This structure is designed to achieve high pump performance due to the controllability of the flexible valve motion and a large amplitude, which increases the kinetic energy given to the liquid. The valve and the slit orifice were confirmed to have a uniform shape. The SEM images also show that the structure has vertical sidewalls across the pattern. The gap between the valve and the sidewalls was measured to be approximately $23 \pm 4 \mu\text{m}$.

4 Experimental setup

The experimental setup for driving the micro-VFP and for the measurement of the pumping performance is shown in Fig. 4. The PM having a magnetic field strength of 0.3 T is

fixed on the shaft of a high-precision mechanical slider (EPF 7M, THK Co., Ltd., Japan) installed on an electromagnetic actuator (ET-132-2, LabWorks Inc., USA) and is vibrated horizontally. The voltage for the electromagnetic actuator is sinusoidal and is generated by a function generator (WF1945B, NF Corp., Japan) with an amplifier (HAS 4014, NF Corp., Japan). The amplitude of the PM is maintained at a constant value of 8 mm, while the frequency of actuation is changed from 5 to 25 Hz. The micro-VFP is fixed to a high-precision stage to control the three-dimensional position relative to the PM. The axis of the vibration and the central position of the PM are set along the microchannel. The vertical distance between the glass substrate and the PM is 0.3 mm, which is experimentally determined so as to maximize the vibration of the valve. From the observation using a microscope, it is confirmed that the deformation of the microchannel due to the valve motion is negligible during the operation of the micro-VFP. The flow outlet and the inlet of the microchannel are, respectively, connected to reservoirs of 1.14 mm in inner diameter for the hydrostatic measurement through two tube connections: 215-mm long polytetrafluoroethylene tubes with an inner diameter of 0.46 mm and 240-mm long flexible tubes with an inner diameter of 1 mm.

Despite the simple design of the micro-VFP, a preliminarily experiment using tap water revealed that the valve sticking to the walls of the slit orifice was a critical issue because of the nature of the PDMS. In order to address this problem, ethanol, which has a lower surface tension, was chosen as a working fluid to reduce the interfacial energy. The density, ρ , of ethanol is 786 kg/m^3 at the temperature of 24 °C. Consequently, smooth periodic motion of the vibrating valve is successfully realized. In a future work, the sticking valve problem can be solved by modifying the shape of the valve, e.g., the edges are modified from straight to curved ones, which reduces the contact area between the

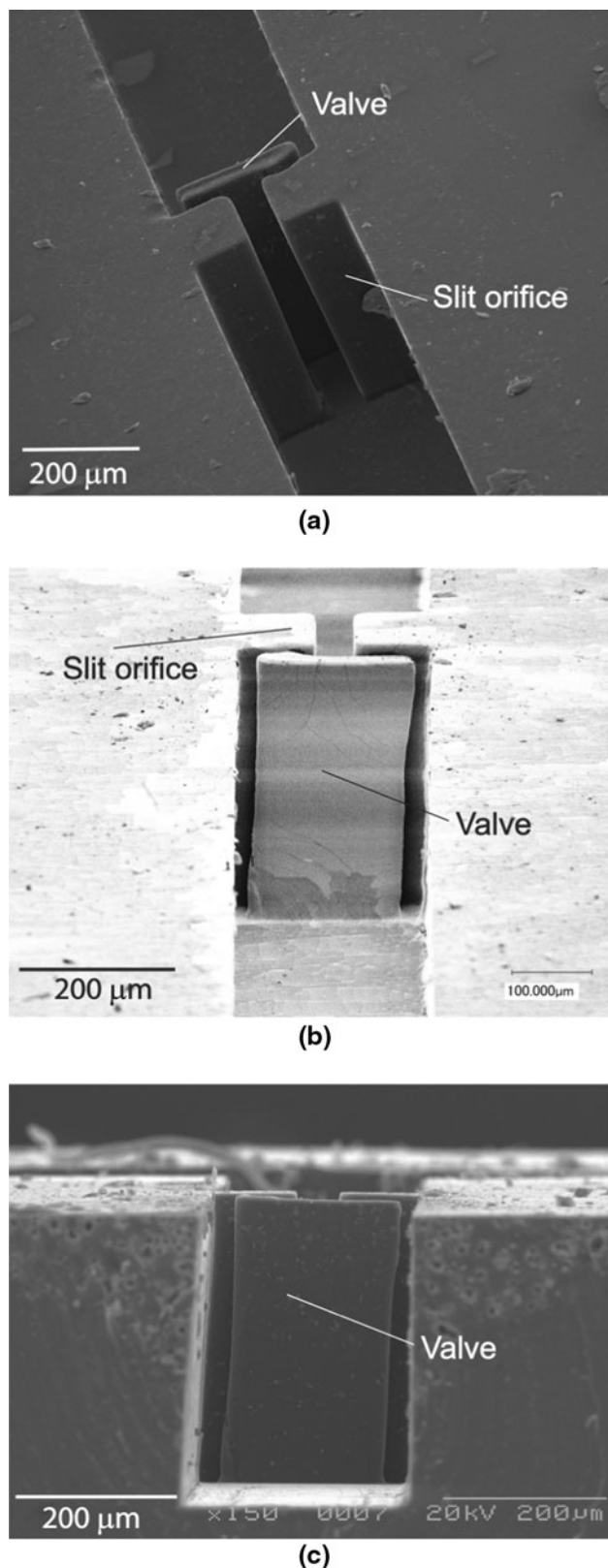


Fig. 3 SEM images of the resultant PDMS structure around a vibrating valve: **a** Birdseye view, **b** 3D view, and **c** front view

valve and the side walls of the microchannel, and enables the micro-VFP applicable to various working fluids. In addition, a specific surface treatment (Tan et al. 2010) can be useful to maintain the hydrophilicity of PDMS surface, which will enable us to use water as a working fluid. The motion of the gas–liquid interface in the reservoirs is observed using a CCD camera (WAT-231S2, Watec Co., Ltd., Japan) and is analyzed by in-house software, which tracks the horizontal gas–liquid interface in real time. The tracking of the interface is achieved by calculating the cross-correlation function for the brightness distribution across the interface. A small amount of red ink is added to the working fluid to enhance the tracking process. The spatial resolution of this measurement is $8.3 \mu\text{m}$ due to the resolution of the present camera system. The flow field in the micro-VFP is visualized using polystyrene fluorescent particles with a diameter of $1.0 \mu\text{m}$ (F8823, Invitrogen™, USA), which are mixed with ethanol at a volume concentration of $1.0 \times 10^{-3} \%$. The flow of the fluorescent particles is observed using a fluorescent stereo microscope (SZX7, Olympus Corp., Japan), which has a relatively large working distance compared with a standard microscope. Since the actuation of the valve occurs from the glass side, we observe the flow from the PDMS side. However, since PDMS has a low transparency compared with glass, in order to obtain a clear image for micro-PIV analysis we used an EMCCD camera (iXon, Andor, USA), which has high sensitivity compared with an ordinary CCD camera. All of the experiments described herein are carried out at a room temperature of $24 \pm 2 \text{ }^\circ\text{C}$ and a relative humidity of $60 \pm 10 \%$.

The principle of the hydrostatic head measurement is shown in Fig. 5. The cross-sectional area of the reservoirs is $1.02 \times 10^{-6} \text{ m}^2$, which is sufficiently wide compared with that of the microchannel of $1.2 \times 10^{-7} \text{ m}^2$, in order to reduce the effect of the time-dependent pressure in the reservoirs. Ethanol is used as the working fluid in the present study in order to easily fill the microchannel with the liquid. However, ethanol evaporates easily, and the interfaces in both reservoirs drop, even without operating the micro-VFP. For this reason, we introduce the assumption that the evaporation rate from both gas–liquid interfaces in the reservoirs is the same. Therefore, the hydrostatic head H generated by the micro-VFP is simply obtained from the difference in height of the liquid interfaces between two reservoirs. The validity of this method is confirmed by the fact that the increase of H is observed only when we operate the micro-VFP. The measurement started under the condition of $H = 0$, and the variation of H is measured as a function of the elapsed time t from the time when the pump started driving. The after load pressure is calculated by ρgH , where g is the gravitational acceleration.

Fig. 4 Schematic diagram of the experimental setup: 1 micro-VFP, 2 permanent magnet, 3 electromagnetic actuator, 4 fluorescent stereo microscope, 5 EMCCD camera, 6 light source, 7 high-precision stage, 8 reservoirs, 9 CCD camera, 10 computer, 11 function generator, 12 amplifier, and 13 mechanical slider

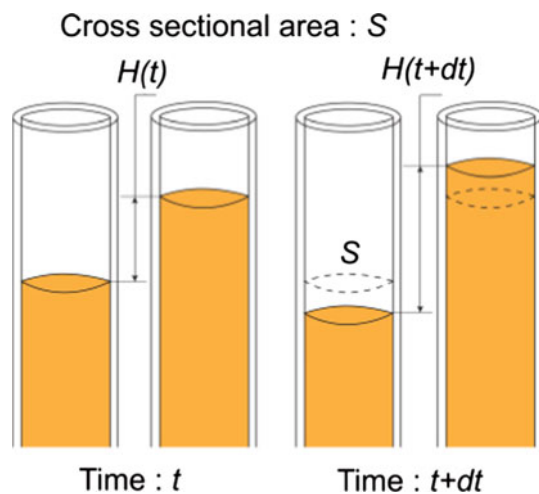
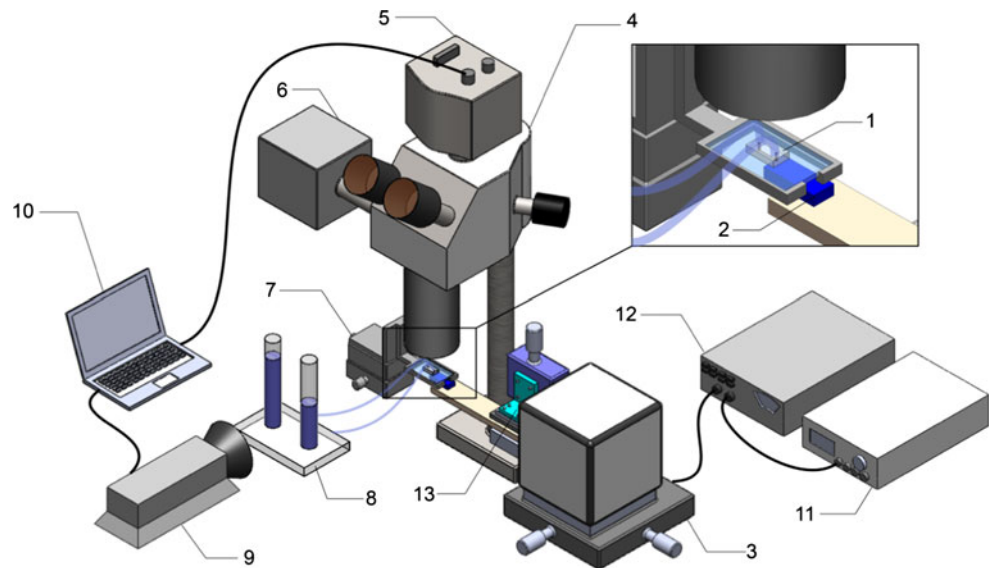


Fig. 5 Principle of hydrostatic head measurement using ethanol as a working liquid

For the micro-PIV analysis, digital images of 512×160 pixels are captured at a frame rate of 110 fps using the EMCCD camera. From a preliminary observation, the flow in the microchannel was found to be symmetric with respect to the x axis but is three-dimensional around the valve. The pumping effect based on the unidirectional flow, which is the time-averaged, may be due to the three-dimensional velocity profile. However, in the present study, as a first step, we evaluated the pumping performance based on the two-dimensional flow field in the x - y plane. We used volume illumination and captured images by setting the focus at the middle plane of the microchannel. The measured depth of field is estimated to be $64 \mu\text{m}$ in the z direction according to the equation given by Meinhart et al. (2000).

5 Results and discussion

5.1 Vibration of the valve

The vibration characteristics of the valve were investigated by mounting a high-speed camera (FASTCAM APX RS, Photron, Japan) on a fluorescent stereo microscope instead of the EMCCD camera. We can take sequential photographs of the phenomena using the high-speed camera through the objective lens and the observation angle can be precisely adjusted. Figure 6a, b shows sequential imaginary illustrations and photographs indicating the side view and top view, respectively, of the valve motion at a frequency of $f = 10$ Hz. The valve is actuated in accordance with the motion of the PM. The valve moves roughly parallel to the sidewall of the microchannel, although the valve sometimes contacts the sidewall, e.g., $t = 80$ ms in Fig. 6b, because of the small clearance between the valve and the sidewall. The distance L between the valve tip and the left edge of the slit orifice is measured in order to characterize the valve motion. Note that the dark color at the valve is due to the magnetic particles. The dark region does not correspond to the valve shadow, but rather to the area with numerous magnetic particles, where the more precise control of the area configuration is quite difficult because of the very small width of $O(100) \mu\text{m}$. Note that the liquid PDMS including magnetic particles is attached to the valve by hand during the fabrication process. The force exerted on the valve is derived from that on the magnetic particles in the valve. Therefore, the distribution of the magnetic particles is an important factor in determining as to how the valve is deformed. Since the cantilever's deformation is related to the fluid-structure

interaction problem, we need to develop a method to precisely control the distribution in our future work. Figure 6c presents the distance L as a function of t . This figure clearly shows that the vibration of the valve is periodic. The reason for the non-sinusoidal change of the distance may be the contact between the valve and the sidewall. The dependence of vibration on the frequency f is investigated using the peak-to-peak amplitude A of the distance, as shown in Fig. 6d. The results indicate that the amplitude A appears to be constant in the frequency range of the present study. Thus, the resonant frequency of the vibrating valve is not in the frequency range used herein. Note that the investigation was carried out at a driving frequency lower than 25 Hz because of the limitation in the actuation of the permanent magnet using the electromagnetic actuator.

5.2 Flow field around the valve

Figure 7a shows the instantaneous velocity field obtained by the micro-PIV analysis under a driving frequency of $f = 10$ Hz. When the PM approaches the valve, the valve deforms from its original position due to the attraction of the magnetic particles in the valve to the magnetic field. The position is decided by the force balance between the magnetic force and the summation of the elastic force and hydrodynamic load. By vibrating the PM the valve vibrates around the new equilibrium point. At $t = 0.0$ ms, the valve is located at the new position of $x = -400$ μm and then starts to move downstream. At $t = 0.0$ – 50.0 ms, while the valve tip moves upstream, the liquid predominantly flows in the same direction as the valve motion, i.e., backflow is induced. At $t = 50.0$ – 100 ms, the liquid flows

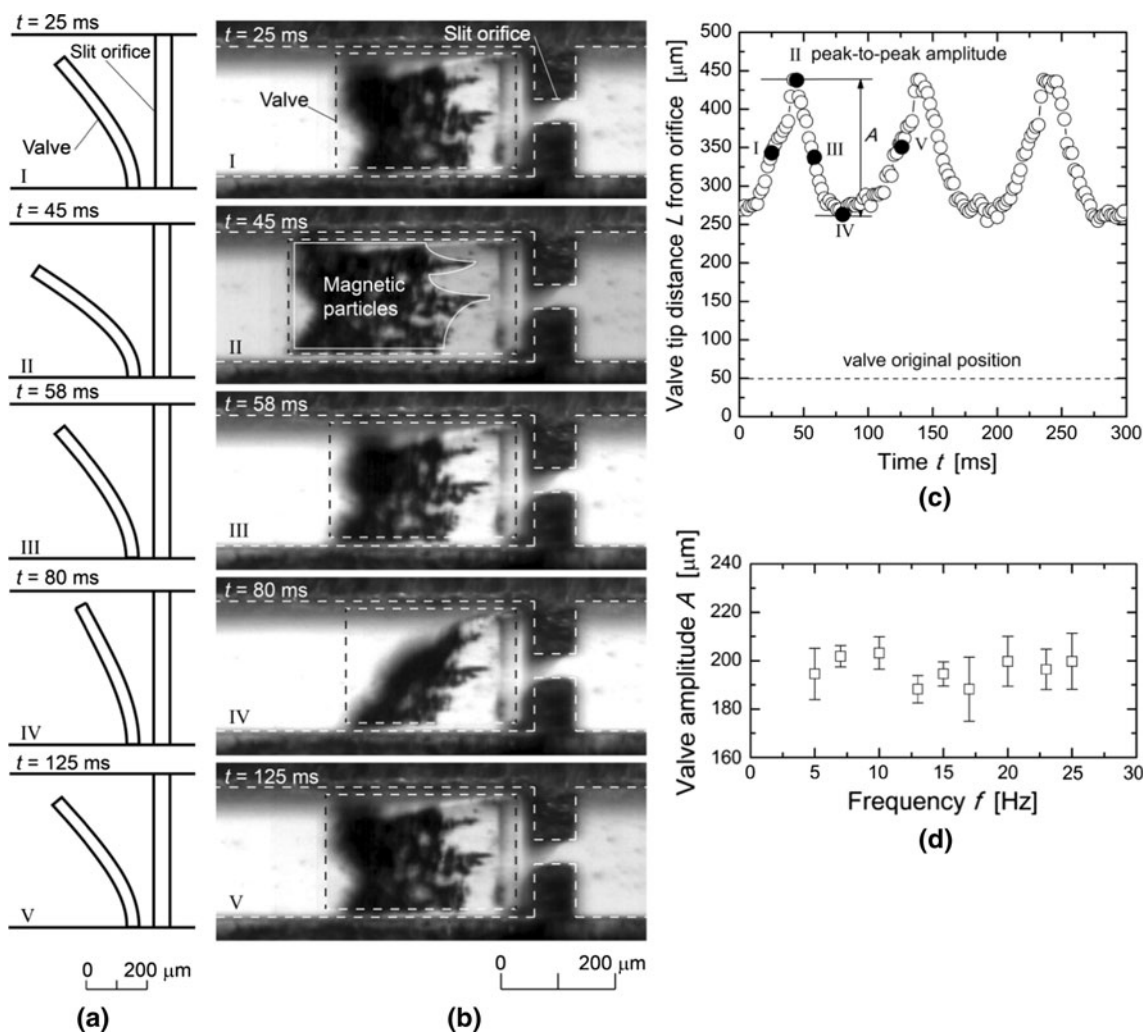


Fig. 6 **a** Sequential and imaginary illustrations showing a side view of the valve motion at $f = 10$ Hz, **b** sequential photographs showing a top view of the valve motion at $f = 10$ Hz, **c** valve tip distance L from

the slit orifice as a function of time t , and **d** valve amplitude A at various frequencies f . Note that the black area in **b** corresponds to that with several magnetic particles, and not to the valve shadow

downstream. When the valve is close to the slit orifice and is moving downstream, e.g., $t = 80.77$ ms in Fig. 7a, pair tip vortices are observed around the valve. The flow is roughly symmetric about the centerline of the microchannel due to the low Reynolds number of $O(0.01)$. These vortices are considered to be induced by the leakage of the liquid through the clearance between the valve and the walls of the microchannel. When the valve moves downstream, the space between the valve and the slit orifice decreases. At this stage, most of the liquid in the space is pushed downstream through the slit orifice. However, part of the volume of the liquid leaks through the clearance, resulting in the generation of pair tip vortices. Although this flow is interesting for enhancing the liquid mixing in the microchannel (Lambert and Rangel 2010), a detailed analysis will be conducted in a future study. Figure 7b shows the experimental path lines in the microchannel, which are obtained through data processing of the micro-PIV results. The flow is completely two-dimensional downstream of the valve. However, upstream, it is difficult to obtain useful information from either the micro-PIV results or the results for the path lines, due to the three-dimensional nature of flow in the upstream.

The relationship between the valve motion and the liquid flow is also evaluated using the spatial mean velocity obtained from the sampling area of $148 \mu\text{m} \leq x \leq 700 \mu\text{m}$, where the flow starts to be fully developed at $x = 148 \mu\text{m}$, as indicated in Fig. 7a. Figure 8 shows the qualitative comparison between the valve tip velocity and the mean velocity of the liquid flow. Note that the valve motion and the velocity field are obtained separately from the different experimental runs. However, the time in the horizontal axis is matched using the elapsed time t from the time when the pump starts. The figure indicates that the velocity of the liquid flow changes in accordance with the valve motion. Although the fully three-dimensional valve motion is simply characterized by the velocity of the valve tip, the valve motion and the mean velocity are in the same phase. From a quantitative viewpoint, however, there is a discrepancy of one order in magnitude between the valve motion and the mean velocity. This may be due to the fact that the leakage of the liquid through the clearance reduces the net flow. Three-dimensional flow measurement should be carried out in the future in order to quantitatively evaluate the flow phenomena and pump efficiency in detail.

5.3 Pumping performance

Figure 9 presents H as a function of time at different driving frequencies. The results indicate that each H increases with time and approaches a certain value. This phenomenon can be understood by the following explanation. Before the operation of the micro-VFP, the

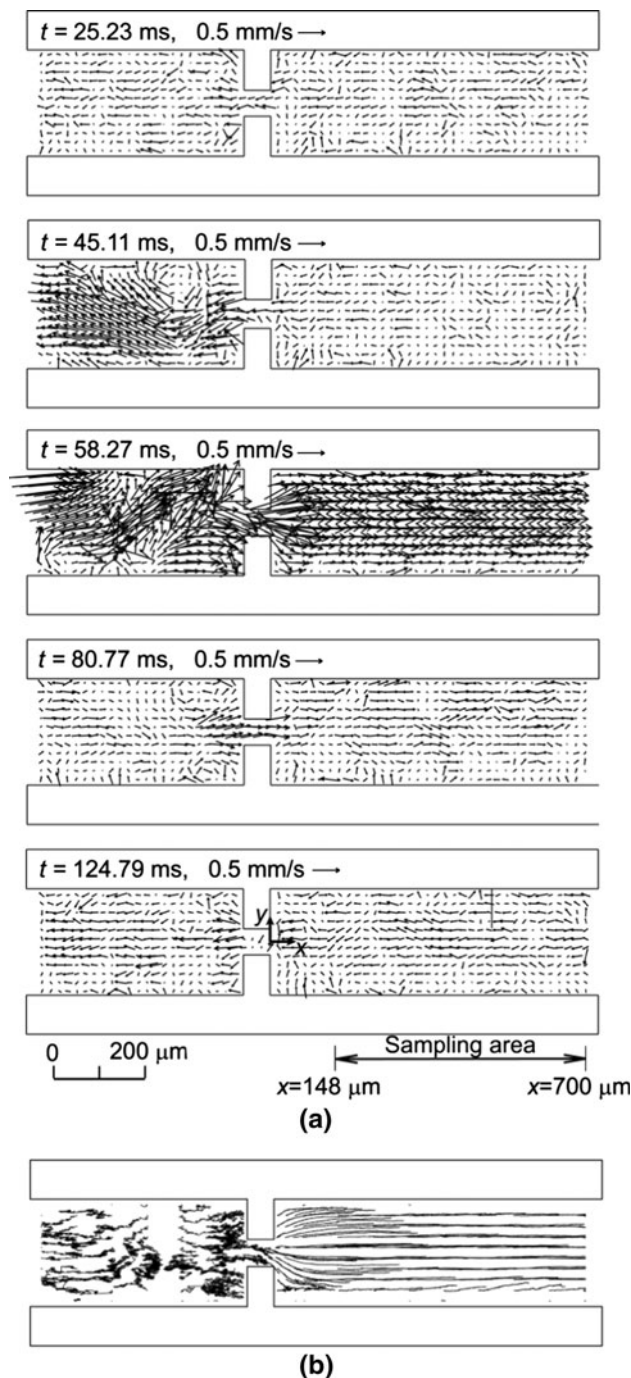


Fig. 7 **a** Instantaneous velocity field obtained by micro-PIV analysis at a frequency of $f = 10$ Hz and **b** experimental path lines in the microchannel

pressures exerted on the inlet and the outlet are balanced and no net flow is generated in the microchannel. When the micro-VFP starts to operate at $t = 0$ s, the liquid in the upstream reservoir is transported downstream. The transported liquid increases the hydrostatic head exerted on the flow outlet and decreased the head in the flow entry. Therefore, at first, H increases with t under the operation of

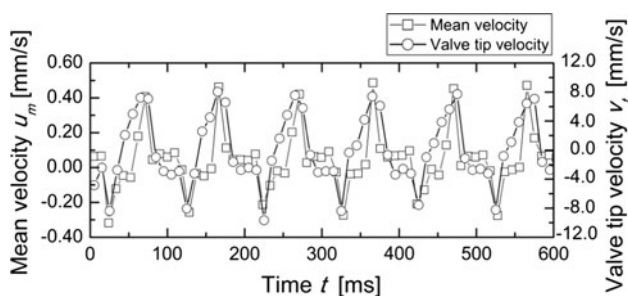


Fig. 8 Relationship between the mean velocity in the sampling area $148 \mu\text{m} \leq x \leq 700 \mu\text{m}$ and the valve tip velocity

the micro-VFP. In addition, the results show that H depends on the driving frequency. The value of dH/dt is related to flow rate Q as $dH/dt = 2Q/S$, where S is the area of the cross section of the reservoir. Therefore, the data is also interpreted such that Q is the highest when the pump starts, i.e., under the zero-head condition, and Q decreases with time, because of the increase of the hydrostatic head. In the steady state, namely $t > 200$ s, the liquid in the upstream reservoir is no longer transported, meaning that there is no net flow in the microchannel. This situation must correspond to the shut-off condition of the pump.

Using the data shown in Fig. 9, the pumping performance of the micro-VFP is evaluated in two limiting cases: $t = 0$ s and the steady state. The value of H at the steady state is used to calculate the shut-off pressure P_s , which is the highest achievable pressure by the micro-VFP at a driving frequency. Figure 10 shows the relationship between P_s and f . The figure shows that P_s increases with the driving frequency f in the range of approximately 1–4 Pa. The highest Q_{max} under the zero-head condition is shown in Fig. 11. It is found that Q_{max} increases with the driving frequency. Furthermore, we compare Q_{max} with the estimated flow rate from the micro-PIV data at

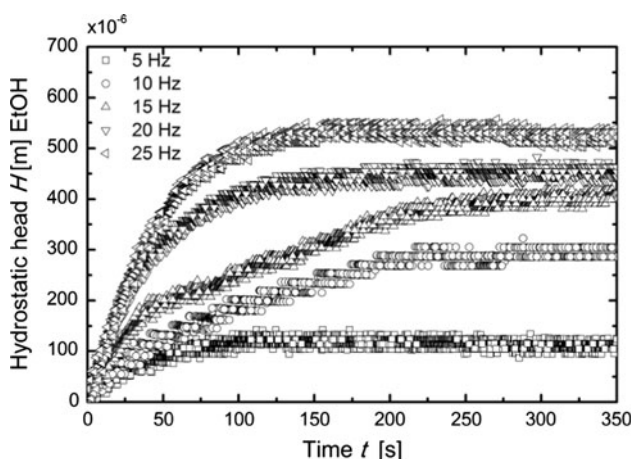


Fig. 9 Variation of hydrostatic head H as a function of time t at various driving frequencies f

$0 \text{ s} \leq t \leq 4.75 \text{ s}$, where H in Fig. 9 appears to increase linearly with t in this time period. Another estimation of Q_{max} is performed by multiplying the cross-sectional area of the microchannel by the spatiotemporally averaged velocity in the sampling area. The comparison appears to be in relatively good agreement, which supports the validity of the assumption that the evaporation from both interfaces was the same and that H generated by the micro-VFP was simply obtained from the difference in height of the liquid interfaces between two reservoirs. The flow rate from the micro-PIV is slightly higher than that obtained from hydrostatic head measurement. This is because the flow rate from the micro-PIV is obtained using only the velocity on the middle plane of the microchannel in the z direction without taking into account the three-dimensional flow field. Based on the data in Figs. 10 and 11, the micro-VFP can realize better pumping performance at a higher driving frequency. The pumping performance is expected to continue to improve by increasing beyond the driving frequency used herein. In the future, we would like to explore the effects of the driving frequency and the vibrating amplitude of the valve on the pumping performance.

Using the micro-VFP, the maximum shut-off pressure P_s and flow rate Q were obtained as $3.8 \pm 0.4 \text{ Pa}$ and $6.38 \times 10^{-12} \pm 3.8 \times 10^{-13} \text{ m}^3/\text{s}$ ($0.38 \pm 0.02 \mu\text{l}/\text{min}$), respectively, at a driving frequency of 25 Hz. These values are relatively small compared to those of previously proposed micropumps. However, from the viewpoint of the flow rate per planform area (Iverson and Garimella 2008), which is calculated as $3.17 \pm 0.17 \mu\text{l}/(\text{min mm}^2)$, the value is relatively large and is in the same range of the

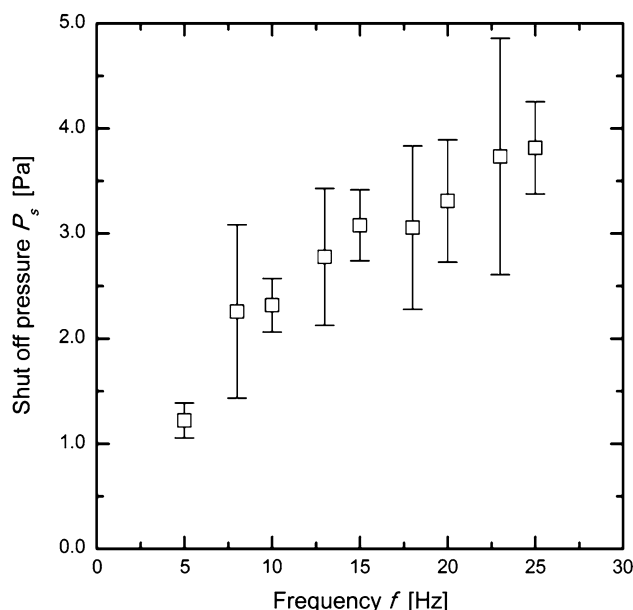


Fig. 10 Shut-off pressure P_s at various driving frequencies f under the steady state

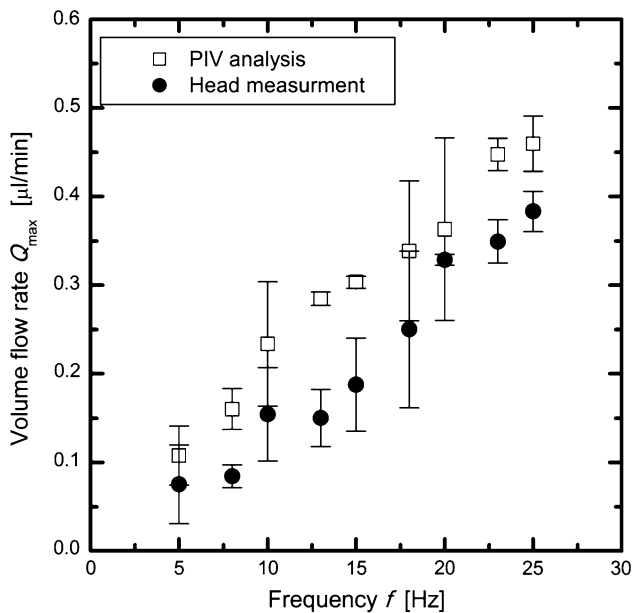


Fig. 11 Maximum flow rate Q_{\max} at various frequencies f under the zero-head condition

conventional diaphragm pumps (Yoon et al. 2007). This means that the micro-VFP can generate a relatively high flow rate for its small size. Furthermore, since the micro-VFP can precisely control the liquid flow at a relatively low flow rate range by changing only the driving frequency, the micro-VFP can be used for emerging biological applications, such as single-molecule analysis (Perkins et al. 1995; Doi et al. 2011; Uehara et al. 2011), glucose monitoring (Hsieh and Zahn 2007; Shintaku et al. 2009), and cell-based assay (Wu et al. 2008), where these applications require the generation of flow ranging from $O(0.01)$ $\mu\text{l}/\text{min}$ to $O(1)$ $\mu\text{l}/\text{min}$ for a long period of time. In addition, the micro-VFP developed herein exhibits no degradation in pumping performance for a cumulative working time of more than 100 h, implying the feasibility of the micro-VFP for practical applications.

6 Conclusions

In the present study, we developed a novel micropump called the micro-VFP. The main advantage of the micro-VFP is that the operation is performed externally only by changing the magnetic field in the vicinity of the vibrating valve without any electrical or mechanical connections. In addition, the micro-VFP is small enough to be incorporated into a relatively tight space because of the simple structure consisting of the valve and slit orifice in the microchannel. The performance of the micro-VFP was investigated under driving frequencies from 5 to 25 Hz by hydrostatic head measurement and two-dimensional flow field analysis

around the valve based on micro-PIV. The results provided the basic design data of performance in the developed micro-VFP and are summarized as follows:

1. A novel micropump, called the micro-VFP, has been developed. In order to demonstrate the applicability of the micro-VFP, a prototype was fabricated using UV lithography and molding in a microchannel with a cross section of $240 \mu\text{m} \times 500 \mu\text{m}$.
2. The results revealed that the pumping performance improved as the driving frequency increased. The maximum shut-off pressure and flow rate were 3.8 ± 0.4 Pa and 0.38 ± 0.02 $\mu\text{l}/\text{min}$, respectively, at a driving frequency of 25 Hz.
3. The hydrostatic head measurement was performed by obtaining the time-dependent height difference of the gas–liquid interfaces between the two reservoirs. The flow rates obtained from the hydrostatic head measurement and from the micro-PIV results were in good agreement. The validity of the measurement methods were confirmed from the viewpoint of practical applications.

Open Access This article is distributed under the terms of the Creative Commons Attribution License which permits any use, distribution, and reproduction in any medium, provided the original author(s) and the source are credited.

References

- Bart SF, Tavrow LS, Mehregany M, Lang JH (1990) Microfabricated electrohydrodynamic pumps. *Sens Actuators A Phys* 21(1–3):193–197. doi:10.1016/0924-4247(90)85037-5
- Doi K, Yonebayashi T, Kawano S (2010) Perturbation theory analysis for electronic response of DNA base pairs. *J Mol Struct: THEOCHEM* 939(1–3):97–105. doi:10.1016/j.theochem.2009.09.046
- Doi K, Ueda M, Kawano S (2011) Theoretical model of nanoparticle detection mechanism in microchannel with gating probe electrodes. *J Comput Sci Technol* 5(2):78–88. doi:10.1299/jcst.5.78
- Hanasaki I, Takahashi H, Sazaki G, Nakajima K, Kawano S (2008) Single-molecule measurements and dynamical simulations of protein molecules near silicon substrates. *J Phys D Appl Phys* 41(9):095301. doi:10.1088/0022-3727/41/9/095301
- Hashimoto H, Hiyana H, Sato R (1994) Development of prototype pump using a vibrating pipe with a valve. *ASME J Fluids Eng* 116:741–745. doi:10.1115/1.2911844
- Hsieh Y-C, Zahn JD (2007) On-chip microdialysis system with flow-through sensing components. *Biosens Bioelectron* 22(11):2422–2428. doi:10.1016/j.bios.2006.08.044
- Inaoka T, Shintaku H, Nakagawa T, Kawano S, Ogita H, Sakamoto T, Hamanishi S, Wada H, Ito J (2011) Piezoelectric materials mimic the function of the cochlear sensory epithelium. *Proc Natl Acad Sci USA* 108(45):18390–18395. doi:10.1073/pnas.1110036108
- Iverson B, Garimella S (2008) Recent advances in microscale pumping technologies: a review and evaluation. *Microfluid Nanofluid* 5(2):145–174. doi:10.1007/s10404-008-0266-8

- Jang J, Lee SS (2000) Theoretical and experimental study of MHD (magnetohydrodynamic) micropump. *Sens Actuators A Phys* 80(1):84–89. doi:[10.1016/s0924-4247\(99\)00302-7](https://doi.org/10.1016/s0924-4247(99)00302-7)
- Kato T, Kawano S, Nakahashi K, Yambe T, Nitta S-i, Hashimoto H (2003) Computational flow visualization in vibrating flow pump type artificial heart by unstructured grid. *Artif Organs* 27(1):41–48. doi:[10.1046/j.1525-1594.2003.07191.x](https://doi.org/10.1046/j.1525-1594.2003.07191.x)
- Kawano S, Yamakami J, Kamijo K, Hashimoto H, Yambe T, Nitta S-i (2001) Computational design of vibration pumping device for artificial heart. *J Pressure Vessel Technol* 123(4):525–529. doi:[10.1115/1.1388009](https://doi.org/10.1115/1.1388009)
- Kawano S, Isoyama T, Kobayashi S, Arai H, Takiura K, Saito I, Chinzei T, Abe Y, Yambe T, Nitta S-i, Imachi K, Hashimoto H (2003) Miniature vibrating flow blood pump using a cross-slider mechanism for external shunt catheter. *Artif Organs* 27(1):73–77. doi:[10.1046/j.1525-1594.2003.07186.x](https://doi.org/10.1046/j.1525-1594.2003.07186.x)
- Kim J-H, Kang CJ, Kim Y-S (2004) A disposable polydimethylsiloxane-based diffuser micropump actuated by piezoelectric-disc. *Microelectron Eng* 71(2):119–124. doi:[10.1016/j.mee.2003.10.005](https://doi.org/10.1016/j.mee.2003.10.005)
- Lambert RA, Rangel RH (2010) The role of elastic flap deformation on fluid mixing in a microchannel. *Phys Fluids* 22(5):052003–052015. doi:[10.1063/1.3410268](https://doi.org/10.1063/1.3410268)
- Liu S, Dasgupta PK (1992) Flow-injection analysis in the capillary format using electroosmotic pumping. *Anal Chim Acta* 268(1):1–6. doi:[10.1016/0003-2670\(92\)85243-y](https://doi.org/10.1016/0003-2670(92)85243-y)
- Manz A, Graber N, Widmer HM (1990) Miniaturized total chemical analysis systems: a novel concept for chemical sensing. *Sens Actuators B Chem* 1(1–6):244–248. doi:[10.1016/0925-4005\(90\)80209-i](https://doi.org/10.1016/0925-4005(90)80209-i)
- Meinhart CD, Wereley ST, Gray MHB (2000) Volume illumination for two-dimensional particle image velocimetry. *Meas Sci Technol* 11(6):809. doi:[10.1088/0957-0233/11/6/326](https://doi.org/10.1088/0957-0233/11/6/326)
- Nagahiro S-i, Kawano S, Kotera H (2007) Separation of long DNA chains using a nonuniform electric field: a numerical study. *Phys Rev E* 75(1):011902. doi:[10.1103/PhysRevE.75.011902](https://doi.org/10.1103/PhysRevE.75.011902)
- Perkins T, Smith D, Larson R, Chu S (1995) Stretching of a single tethered polymer in a uniform flow. *Science* 268(5207):83–87. doi:[10.1126/science.7701345](https://doi.org/10.1126/science.7701345)
- Peter W (2005) Micropumps—past, progress and future prospects. *Sens Actuators B Chem* 105(1):28–38. doi:[10.1016/j.snb.2004.02.033](https://doi.org/10.1016/j.snb.2004.02.033)
- Shintaku H, Kuwabara T, Kawano S, Suzuki T, Kanno I, Kotera H (2007) Micro cell encapsulation and its hydrogel-beads production using microfluidic device. *Microsyst Technol* 13(8):951–958. doi:[10.1007/s00542-006-0291-z](https://doi.org/10.1007/s00542-006-0291-z)
- Shintaku H, Imamura S, Kawano S (2008) Microbubble formations in MEMS-fabricated rectangular channels: a high-speed observation. *Exp Thermal Fluid Sci* 32(5):1132–1140. doi:[10.1016/j.expthermflusci.2008.01.004](https://doi.org/10.1016/j.expthermflusci.2008.01.004)
- Shintaku H, Tataru Y, Kawano S (2009) Droplet transportation on vertical parallel electrodes using electrowetting and interfacial oscillation. *J Fluid Sci Technol* 4(3):636–647. doi:[10.1299/jfst.4.636](https://doi.org/10.1299/jfst.4.636)
- Shintaku H, Yonemura T, Tsuru K, Isoyama T, Yambe T, Kawano S (2010) Oxygenation to bovine blood in artificial heart and lung using vibrating flow pump: experiment and numerical analysis based on non-Newtonian model. *J Fluid Sci Technol* 5(2):292–304. doi:[10.1299/jfst.5.292](https://doi.org/10.1299/jfst.5.292)
- Stone HA, Stroock AD, Ajdari A (2004) Engineering flows in small devices: microfluidics toward a lab-on-a-chip. *Annu Rev Fluid Mech* 36:381–411. doi:[10.1146/annurev.fluid.36.050802.122124](https://doi.org/10.1146/annurev.fluid.36.050802.122124)
- Tan SH, Nguyen N-T, Chua YC, Kang TG (2010) Oxygen plasma treatment for reducing hydrophobicity of a sealed polydimethylsiloxane microchannel. *Biomicrofluidics* 4(3):32204–32208. doi:[10.1063/1.3466882](https://doi.org/10.1063/1.3466882)
- Uehara S, Shintaku H, Kawano S (2011) Electrokinetic flow dynamics of weakly aggregated lambda DNA confined in nanochannels. *J Fluids Eng* 133(12):121203–121208. doi:[10.1115/1.4005343](https://doi.org/10.1115/1.4005343)
- van Lintel HTG, van De Pol FCM, Bouwstra S (1988) A piezoelectric micropump based on micromachining of silicon. *Sens Actuators* 15(2):153–167. doi:[10.1016/0250-6874\(88\)87005-7](https://doi.org/10.1016/0250-6874(88)87005-7)
- Wu M-H, Huang S-B, Cui Z, Cui Z, Lee G-B (2008) Development of perfusion-based micro 3-D cell culture platform and its application for high throughput drug testing. *Sens Actuators B Chem* 129(1):231–240. doi:[10.1016/j.snb.2007.07.145](https://doi.org/10.1016/j.snb.2007.07.145)
- Yambe T, Yoshizawa M, Tanaka A, Abe K-i, Kawano S, Matsuki H, Maruyama S, Amae S, Wada N, Kamiyama T, Takagi T, Luo R, Hayashi J, Kovalev YA, Sha DXD, Nanka S, Saijo Y, Mibiki Y, Shibata M-i, Nitta S-i (2003) Recent progress in artificial organ research at Tohoku University. *Artif Organs* 27(1):2–7. doi:[10.1046/j.1525-1594.2003.07181.x](https://doi.org/10.1046/j.1525-1594.2003.07181.x)
- Yoon JS, Choi JW, Lee IH, Kim MS (2007) A valveless micropump for bidirectional applications. *Sens Actuators A Phys* 135(2):833–838. doi:[10.1016/j.sna.2006.08.017](https://doi.org/10.1016/j.sna.2006.08.017)